

Characteristics of the Multi-Telescope Coincidence Trigger of the HEGRA IACT System

N. Bulian, A. Daum, G. Hermann, M. Heß, W. Hofmann,
H. Lampeitl, G. Pühlhofer, C. Köhler, M. Panter, M. Stein

*Max-Planck-Institut für Kernphysik, P.O. Box 103980, D-69029 Heidelberg,
Germany*

G. Börst, G. Rauterberg, M. Samorski, C. Sauerland,
W. Stamm

Universität Kiel, Inst. für Kernphysik, Olshausenstr.40, D-24118 Kiel, Germany

Abstract

The HEGRA-collaboration is operating a system of imaging atmospheric Cherenkov telescopes to search for sources of TeV- γ -rays. Air showers are observed in stereoscopic mode with several telescopes simultaneously. To trigger the telescope system a versatile two-level trigger scheme has been implemented, which allows a significant reduction of the energy threshold with respect to single telescopes. The technical implementation of this trigger scheme and the performance of the trigger system are described. Results include the dependence of single- and multi-telescope trigger rates on the trigger thresholds, on the orientation of the telescopes, and on the type of the primary particle.

1 Introduction

Imaging atmospheric Cherenkov telescopes (IACT) [1] have proven to be the most powerful instruments in TeV- γ -ray astronomy. The high sensitivity of these instruments results from the large effective collection area, governed by the size of the light pool of air showers, and from an effective hadron suppression [2], achieved by the imaging technique. Further improvements of the Cherenkov technique can be obtained by coupling several telescopes to a system for stereoscopic observations of air showers.

The HEGRA-collaboration has installed such a stereoscopic system during the last two years and first measurements show very encouraging results [3,4].

The HEGRA IACT system is located on the Canary Island of La Palma, at the Observatorio del Roque de los Muchachos of the Instituto Astrofisico de Canarias, at a height of about 2200 m asl. In its final form, the HEGRA IACT array will consist of five identical telescopes with 8.5 m² mirror area, 5 m focal length, and 271-pixel cameras [5] with a pixel size of 0.25° and a field of view of 4.3°. Four telescopes (CT2, CT4, CT5, CT6) are arranged in the corners of a square with roughly 100 m side length, and one telescope (CT3) is located in the center of the square. At this time, only four of the telescopes (CT3, CT4, CT5, CT6) are included in the IACT system; the last telescope (CT2, at one corner of the square) is still equipped with an older camera and is operated independently. The cameras are read out by Flash-ADCs with 120 MHz sampling rate and 34 μ s memory depth.

Triggering of such an IACT system is rather more complex than for single IACTs. Given that the stereoscopic analysis requires good images in at least two telescopes, already at the trigger level a multi-telescope coincidence is requested. Such a coincidence trigger will very effectively suppress background triggers generated by the light of the night sky and by local muons, allowing to significantly reduce the trigger threshold and hence the energy threshold. A telescope coincidence is also expected to enhance the ratio of γ -ray triggers to cosmic-ray events.

In this paper, we give an overview of the characteristics of the trigger of the HEGRA IACT array, with emphasis on trigger rates and their dependence on the various parameters; the technical implementation is also summarized briefly.

2 The two-level trigger system

The trigger system of the HEGRA IACTs is designed as a two-level system. First, for each telescope a ‘local’ trigger is derived by requiring that signals in a minimum number of pixels (typically 2) exceed a given threshold, optionally imposing additional topological constraints emphasizing the compactness of shower images. The pattern of trigger pixels is latched for later use. This first local trigger level operates essentially without deadtime, allowing in extreme cases local trigger rates in the MHz range. The local trigger electronics is housed in a container near each telescope, together with the Flash-ADC digitizers and a CPU for readout and data buffering as well as for telescope control and monitoring. The local telescope trigger signals are routed to a central station. There, in the second ‘global’ trigger level, several telescopes are required to trigger in coincidence. During the about 1 μ s required for the propagation and processing of trigger signals, event data are stored locally in the Flash-ADC memory; only after a global trigger, the continuous conversion

is stopped and data are read out. Since the full time history of the last $34\ \mu\text{s}$ for all pixels of all telescopes is stored, event data can be collected irrespectively of whether a given telescope contributed to the global trigger or not.

To provide maximum flexibility, all relevant parameters, such as the pattern of pixels included in the trigger, the thresholds, and the coincidence levels are under computer control. This feature allows the trigger system to automatically adapt to changing conditions, such as bright stars moving through the field of view. The extensive use of configuration files and history files ensures that trigger conditions are well documented and reproducible.

The local trigger electronics at each telescope relies primarily on three different types of logic modules: the Discriminator-Monitor Cards (DMC), the majority unit, and the topological trigger unit.

Signals from the camera PMTs are amplified in the camera by a factor 16 and are then routed via 22 m of RG178-cable to the DMCs and the Flash-ADCs. The amplifiers in the camera also serve to convert the average DC current from the PMTs into DC voltage levels, which are superimposed to the AC-coupled signals [5]. Typical PMT signals arriving at the DMC cards have a signal level of 1.2 mV/photoelectron and 6 ns pulse width (FWHM). Each DMC (Fig. 1) serves 16 analog input channels. For each channel, it provides an input amplifier of gain 3 and a discriminator. Discriminator thresholds can be set independently via VME, with a threshold up to 80 mV (referring to the level at the DMC input), equivalent to a range of roughly 0 to 70 photoelectrons. Discriminator outputs are available both individually on front-panel connectors, and as 8-channel summed outputs, which provide a voltage proportional to the number of triggered pixels. Channels can be individually disabled via VME. This feature is used to exclude single channels dynamically from the trigger if, e.g., a bright star is imaged into the pixel. The length of the discriminator output signals is hardware-adjustable, and is set to 17 ns. In order to preserve the information on triggered pixels, the discriminator outputs can be latched on the DMC, by applying an external ‘hold’ signal when the telescope triggers. Since the latch signal will only arrive with a certain delay caused by the trigger electronics and cables, the input signals to the VME-readable latches are extended to 100 ns length by a monoflop, to guarantee sufficient overlap. The DMC contains furthermore a multiplexed scaler to monitor pixel rates, and ADCs for the measurements of the average PMT currents.

The 8-channel summed outputs from the DMCs - 34 in total to serve the 271 pixels of a camera - are routed to the majority unit, where the outputs of all DMCs are summed up and discriminated with a software adjustable threshold, corresponding to the minimal number of pixels required for the trigger. A minimal overlap of the input signals of 3 ns is needed, resulting in an effective

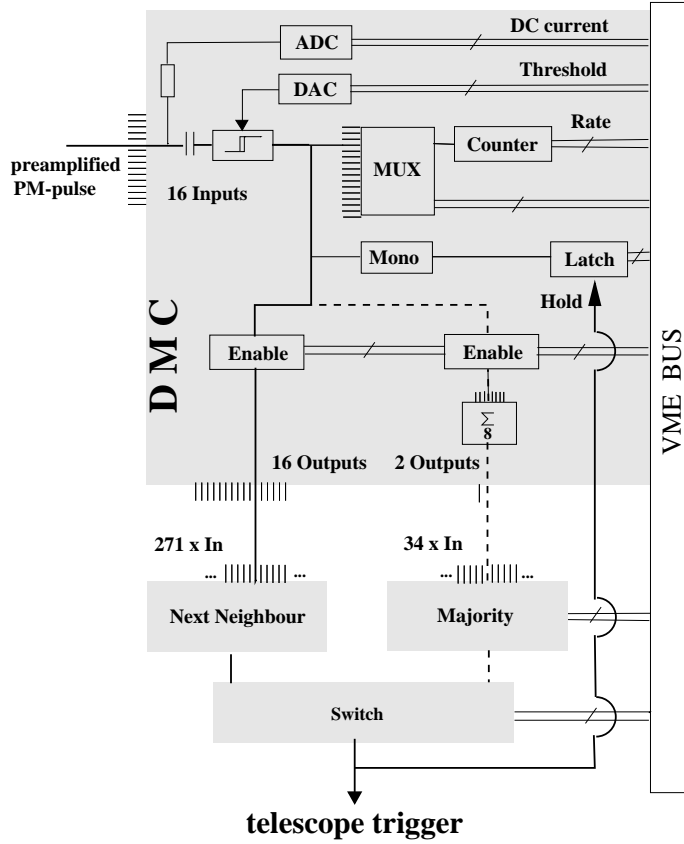


Fig. 1. Configuration of the trigger electronics, emphasizing the function of the Discriminator-Monitor Cards (DMCs), with the trigger discriminators, gated trigger outputs and latches, and monitoring of PMT currents as well as trigger rates.

coincidence window of 14 ns. The usual trigger condition requires the coincidence of two pixels; Monte Carlo studies showed that for the given pixel size of 0.25° , such a two-pixel coincidence is more efficient in rejecting backgrounds than, say, a three-pixel coincidence with lower pixel thresholds. The majority unit again contains a scaler to monitor trigger rates, and additional inputs for auxiliary triggers, which can be enabled under VME control.

An alternative ‘next-neighbor’ (NN) trigger is provided by the topological trigger unit, which receives as input the 271 individual discriminator outputs, and which requires at least two triggering pixels to be neighbors. The logic is implemented using programmable gate arrays; the typical trigger decision time of 20 ns is comparable to that of the majority unit. The required minimum overlap of the input signals is 3 ns. With this logic, accidental background triggers, caused by the light of the night sky, are reduced by a factor of about 48, while over 95% of the compact γ -ray images are kept [6]. The improved suppression of accidental triggers allows to reduce pixel trigger thresholds and hence the energy threshold of the telescope.

The NN trigger signal is fed back into one of the additional trigger inputs of the majority unit; via VME, either this external trigger or the internal majority signal can be switched to the trigger outputs, which also generate the hold signals for the latch registers on the DMCs. For normal observations, the NN trigger is enabled; the majority trigger is nowadays used only for special studies and tests.

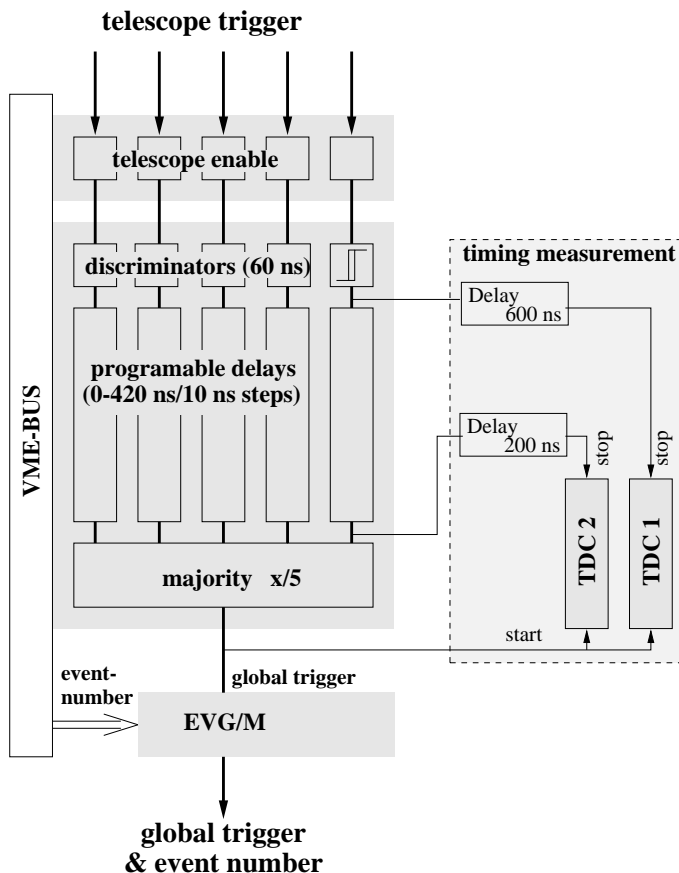


Fig. 2. Sketch of the central trigger logic of the HEGRA IACT array, and of the TDCs used to monitor trigger timing. The modules and connections used for the calibration of the TDCs are not shown.

The local trigger signals of each telescope are routed to the central station using cables of identical length. There, the global trigger for the IACT system is derived.

The main task of the central station is to generate a trigger if at least a preset number of telescopes, typically two, have triggered within a given coincidence time. In order to allow a short window for these inter-telescope coincidences, differences in the arrival times of the Cherenkov light front at the individual telescopes have to be compensated. With a separation of up to 140 m between telescopes, arrival times of trigger signals may differ by almost 400 ns for showers at angles of 60° from the zenith. Key element of the central station is therefore a VME board with five computer-controlled delay units, feeding

a majority discriminator (Fig. 2). The delays are implemented as switched delay lines, adjustable in steps of 10 nsec. The delay settings are updated continuously while a source is tracked across the sky. The width of the inter-telescope coincidence window is set to a conservative value of 70 ns. Trigger arrival times both before and after the delay are monitored with TDCs. Fig. 3 shows the relative timing of trigger signals from two telescopes (CT3 and CT5), with a width of about 6 ns rms. Apart from the finite step size of the delay adjustments, a number of effects contribute to this width. The intrinsic time resolution of the telescope signals is of order 1 ns and is negligible in this context. More important is the fact that the axes of triggered showers may deviate by as much as 2° from the telescope axis (limited essentially by field of view of the cameras). Correspondingly, given the 75 m spacing of the two telescopes, arrival delays may differ by up to 7 ns from their nominal values. In addition, since the Cherenkov light front resembles a spherical wave front rather than a plane wave, the relative timing may vary by another 5 ns depending on the location of the triggered telescopes relative to the shower core.

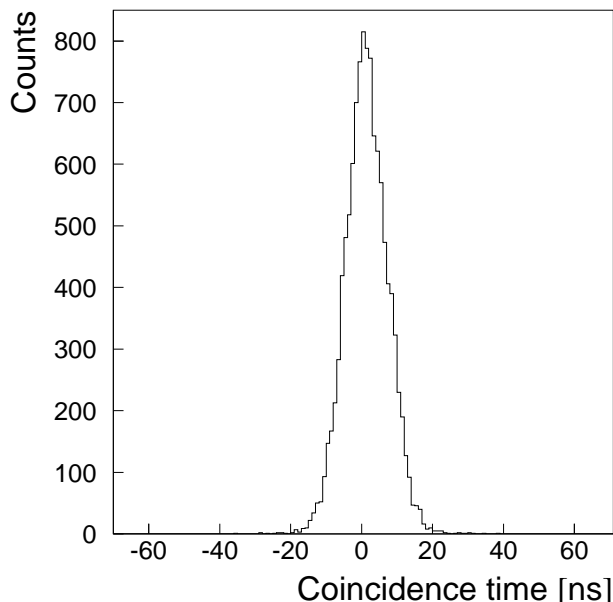


Fig. 3. Distribution in the differences of the arrival times of triggers from the two telescopes CT3 and CT5, after approximate compensation of the differences in propagation delay. The spacing between the telescopes is 75 m.

The global trigger signal is then sent to all telescopes of the system by a custom unit (EVG/M in Fig. 2), which appends to the basic trigger signal an event number used to synchronize events. This unit also provides the option to calibrate the cable delays between the central station and the telescopes. The receiver units trigger, via an interrupt, the readout of the Flash-ADCs by the

local CPUs at each telescope. During interrupt handling, further triggers are disabled, but the receiver units keep count of global triggers arriving during this deadtime. Since the processing time of individual telescopes may vary, the deadtime of the telescopes is largely, but not completely correlated. At typical trigger rates of 15 Hz, the global system dead time is below 5 %. About 97% of the events are complete in the sense that all telescopes are read out; in the remaining 3%, at least one telescope was still busy processing previous triggers.

3 Cosmic-ray trigger rates

As part of the commissioning of the IACT system, trigger rates at the various levels - pixel rates, local telescope trigger rates, and global system trigger rates - were studied as a function of pixel trigger thresholds. For these measurements, the telescopes were pointed at a dark region of the sky near the zenith. Using a pulsed light source in the center of the mirror dish, the cameras were flat-fielded by adjusting the high-voltage of the individual PMTs. To determine offset voltages of the discriminators, thresholds were scanned, watching the discriminators toggle once the threshold crossed the offset. Offsets determined by this technique vary by a few mV; discriminator thresholds quoted in the following are offset-corrected.

From the width of the distribution of digitized amplitudes of the laser calibration pulses one can, after corrections for the width of the single-photoelectron peak and for intensity fluctuations of the laser, determine the average number of photoelectrons per pixel, and hence the pulse height equivalent to a single photoelectron. An average single-photoelectron signal corresponds to a voltage at the discriminator of about 1.2 mV. We note, however, that the PMTs are adjusted to provide a fixed signal for a given (relatively large) amount of light; this means that the product of PMT quantum efficiency, collection efficiency, PMT gain and electronics gain is constant, but not necessarily the PMT gain and electronics gain alone, which determine the single-photoelectron signal.

Fig. 4 shows the distribution of pixel trigger rates for each of the CT cameras, for a pixel trigger threshold of 8 mV. Rates vary significantly both from pixel to pixel, and between telescopes. As discussed elsewhere [7,8], the prime source of single-pixel triggers under typical IACT conditions are not genuine multi-photoelectron events (the rate of which should be pixel-independent), but instead large afterpulses of single-photoelectron events, generated when an atom of the residual gas in the PMT is ionized and accelerated towards the photocathode, where it knocks out further electrons. The rate of such afterpulses varies strongly between individual PMTs. Telescopes CT3 and CT4 differ from CT5 and CT6 by about a factor of 3 in the mean pixel rate at a

given threshold; this difference is not too surprising, since PMTs were grouped according to the high voltage required for a given gain, and the cameras of CT3 and CT4 require slightly higher average operating voltages, compared to CT5 and CT6. The afterpulse rate, on the other hand, depends strongly on the voltage applied between photocathode and first dynode [7]. Fig. 5 shows the average pixel trigger rates of the telescopes CT3 through CT6, as a function of the trigger thresholds.

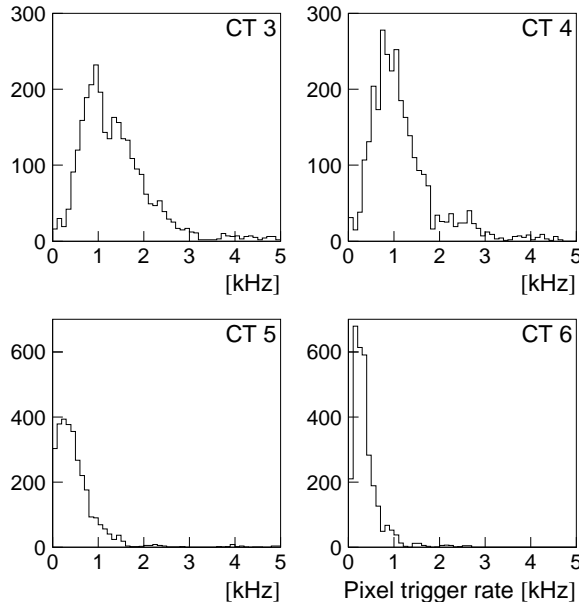


Fig. 4. Distribution of the trigger rate of individual pixels at a fixed pixel threshold of 8 mV, for each of the telescopes. For each pixel, multiple rate measurements are contained in the plot.

The two-pixel coincidence rate is displayed in Fig. 6(a), for the majority trigger unit. It displays two separated regimes. At high thresholds, above about 18 mV, or 15 photoelectrons, random pixel coincidences are rare and the rate of events is determined by genuine cosmic-ray triggers. The trigger rates follow a power law spectrum (see Table 1), and all telescopes behave almost identical. Small rate differences between telescopes at the level of 10% are most likely related to the differences in the age and hence reflectivity of the mirrors (measured reflectivities vary between 81% and 85% [9]), and also to differences in the quality of the mirror alignment. The power-law slope of the rate curve is slightly smaller than the cosmic-ray integral spectral index; this behaviour is reproduced by Monte Carlo simulations and results from the slightly non-linear relation between the shower energy and the density of Cherenkov light on the ground, and from the influence of fluctuations. At lower thresholds, coincidence rates rise steeply with decreasing thresholds, and are dominated by random coincidences. In this regime, significant differences between the

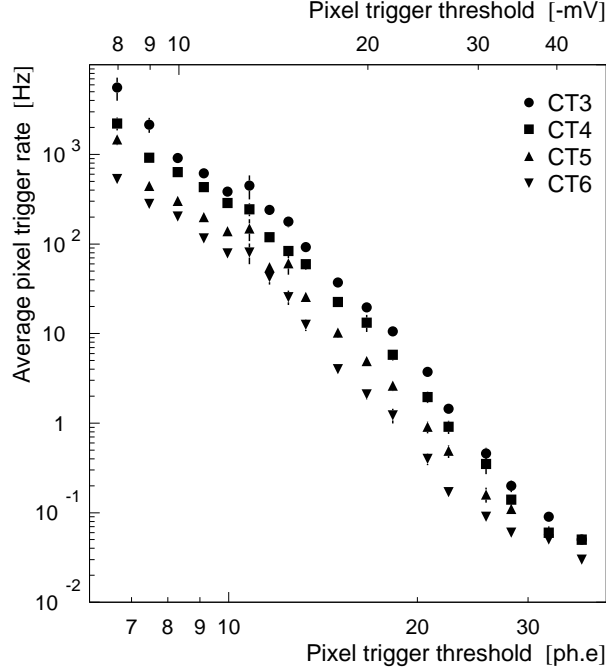


Fig. 5. Trigger rate of single pixels, averaged over all pixels of a telescope, as a function of the trigger threshold both in mV and in photoelectrons.

telescopes reflect the differences in the mean PMT trigger rates; the measured rates are consistent with the expected random rates, as derived using the measured pixel trigger rates and a 14 ns coincidence window.

Trigger condition	Rate at 15 mV pixel threshold	Spectral index
Single telescope, majority	9.7 ± 1.3 Hz	1.28 ± 0.18
Single telescope, NN trigger	9.6 ± 0.8 Hz	1.35 ± 0.09
≥ 2 telescopes, majority	7.9 Hz	1.45
≥ 3 telescopes, majority	4.1 Hz	1.35
4 telescopes, majority	1.7 Hz	1.42
≥ 2 telescopes, NN trigger	7.2 Hz	1.33
≥ 3 telescopes, NN trigger	3.8 Hz	1.34
4 telescopes, NN trigger	1.6 Hz	1.45

Table 1

Trigger rate and effective spectral index for different trigger conditions, derived using a power-law fit to the measured rates as a function of threshold in the regions where rates are dominated by genuine air showers. Rates quoted represent the fit value for a common pixel threshold of 15 mV. The errors quoted for the single-telescope values represent the variation of values between telescopes. Statistical errors on the rates are generally below 0.1 Hz, and errors on the power-law slope are below 0.05.

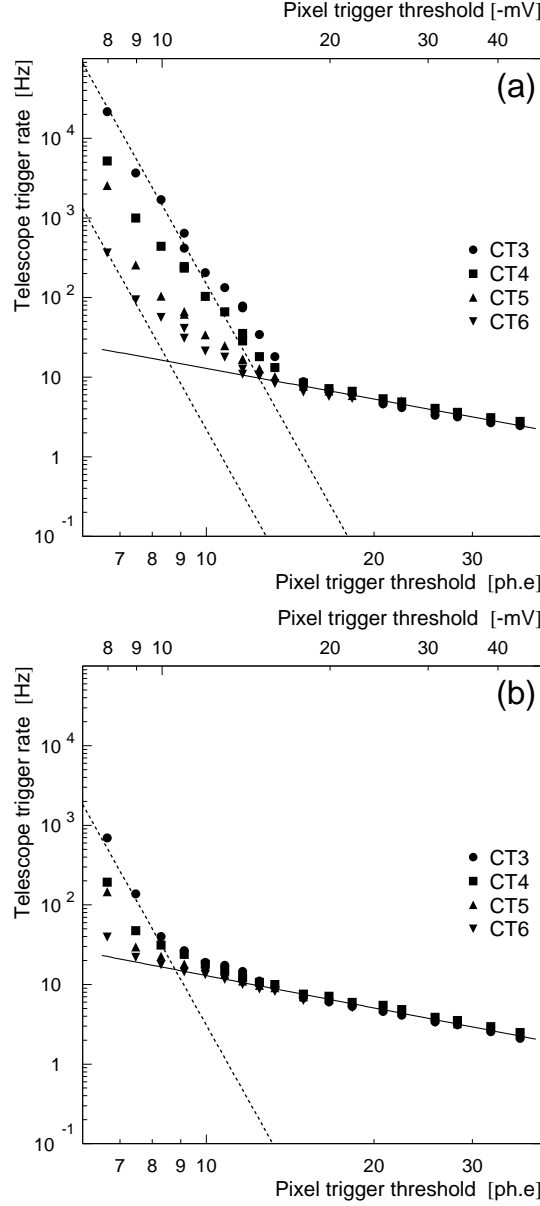


Fig. 6. (a) Two-pixel coincidence rate of the different telescopes, as a function of the trigger threshold both in mV and in photoelectrons. Also shown are the random-coincidence rates for CT3 (upper dashed line) and CT6 (lower dashed line) calculated from the measured pixel trigger rates assuming a coincidence time of 14 ns. The full line represents a power-law fit to the data points for larger thresholds. (b) Same for the next-neighbor trigger, which requires that at least two of the triggered pixels are direct neighbors. The dashed line indicates the random rate for CT3.

The next-neighbor (NN) trigger unit should effectively suppress random coincidences by restricting the number of possible pixel combinations. Fig. 6(b) shows the corresponding rates. Indeed, the onset of a significant rate of random triggers occurs at significantly lower thresholds of around 10 mV to 15

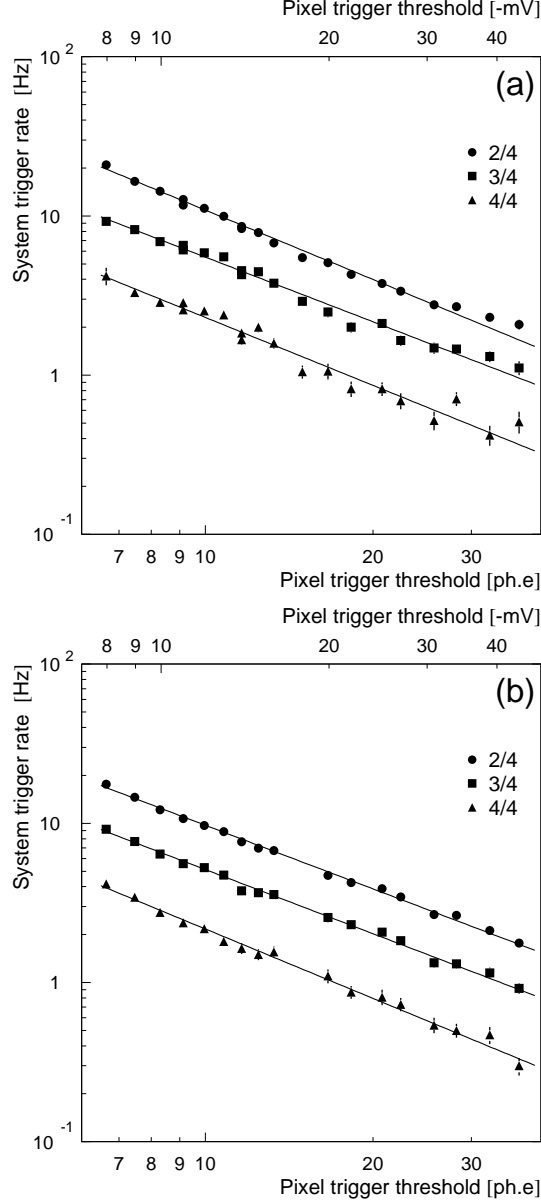


Fig. 7. (a) Two-, three- and four-telescope coincidence rate, as a function of the trigger threshold both in mV and in photoelectrons, using the any-two-pixel (majority) trigger to derive telescope triggers. (b) Same using the next-neighbor (NN) trigger.

mV, or 8 to 12 photoelectrons. For high thresholds, trigger rates are close to the rates with the majority unit (see also Table 1), indicating minimal losses ($\leq 10\%$) even for the more diffuse proton images.

The any-two-pixel or next-neighbor coincidence signals are sent to the central trigger station, which checks for coincidences with other telescopes. Two-, three- and four-telescope trigger rates are summarized in Fig. 7, for the two-pixel majority trigger and for the next-neighbor trigger. For all conditions

studied, there is no evidence for the onset of a significant contribution of random triggers. Rate estimates show, indeed, that for the two-telescope, any-two-pixel trigger the rate of random telescope coincidences amounts to about 30% of the total rate at the lowest threshold value; for the next-neighbor logic the random fraction drops to about a fraction of a percent. With such a multi-telescope coincidence, random coincidences do no longer play a significant role in the choice of trigger thresholds, and other factors enter, such as the stability of the electronics for such low thresholds, and the fact that images with only a few 10 photoelectrons provide limited information. Presently, the HEGRA IACT system is operated with 8 mV pixel thresholds and a two-telescope coincidence requirement.

The rates and effective spectral index for the different cases are included in Table 1. The spectral index, the ratios between 1, 2, 3 and 4-telescope coincidence rates and – within the 10% to 20% uncertainty in the sensitivity of the telescopes – also the absolute rates are reproduced by Monte Carlo simulations; a detailed comparison of measured and predicted rates and of event characteristics will be the subject of a forthcoming paper.

4 Dependence of rates on telescope alignment

In a stereoscopic system of IACTs, the relative orientation of the telescopes enters as an additional parameter. Two options are frequently discussed:

- one can either align the axes of all telescopes parallel, or
- recognizing that most of the Cherenkov light emerges around the shower maximum, at a finite height of $h \approx 6$ km above the telescopes (for typical HEGRA conditions), one can tilt the telescopes inward such that they point to the same spot at the height of the shower maximum.

In a somewhat simplified picture, two conditions need to be fulfilled for a telescope to trigger: the telescope needs to be located in the Cherenkov light pool, and the shower maximum needs to be within the field of view. Tilting two telescopes towards each other by about $d/h \approx 0.7^\circ$ to 1° should provide the maximum overlap of the fields of view and hence the maximum trigger rate. Here, $d \approx 70$ m to 100 m is the telescope spacing.

To verify this expectation, coincidence rates of the two telescopes CT3 and CT4 were measured as a function of their relative pointing. Fig. 8(a) shows the coincidence rate as a function of the tilt along the direction connecting the two telescopes. One finds indeed that the maximum rate is achieved when the telescopes are slightly canted towards each other; the dependence of coincidence rates as a function of the tilt is reproduced remarkably well by a

simple geometrical model, calculating the overlap of the circular fields of view at the height of the shower maximum (dashed line). A tilt perpendicular to the connecting line of course yields a symmetrical curve (Fig. 8(b)).

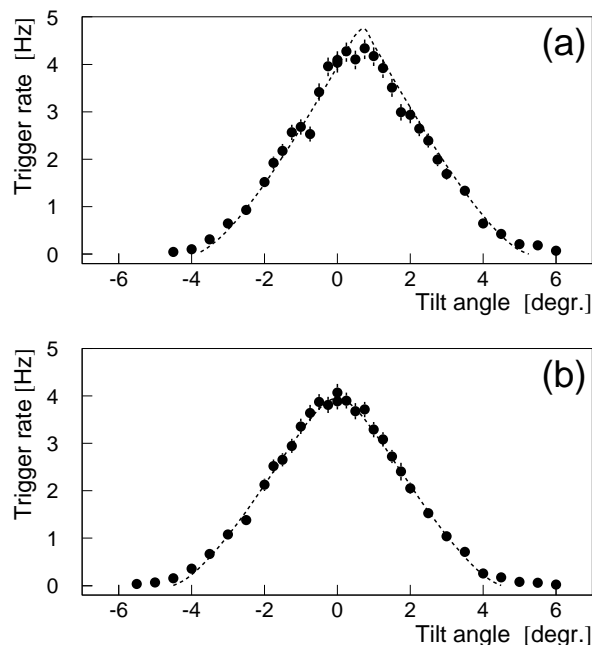


Fig. 8. Coincidence rates between telescopes CT3 and CT4 as a function of the relative alignment of the telescope axes. In (a), the axes are tilt along the direction connecting the telescopes; a positive tilt means that the telescopes look towards each other. In (b), the telescopes are tilt perpendicular to the connecting line. The dashed curves correspond to the geometrical overlap of the camera fields of view at a height of 6.3 km above the observation level.

One also notices that the relative alignment of the telescopes is not particularly critical; from the point of view of trigger rates, deviations up to a fraction of a degree are tolerable. Given the modest resulting losses, the HEGRA system telescopes have so far been operated with parallel axes, for operational convenience.

5 Dependence of rates on the zenith angle

For future studies of systematics, in particular concerning observations at large zenith angles, the dependence of single-telescope and multi-telescope cosmic-ray trigger rates on the zenith angle is of interest. Fig. 9 shows the relevant data. In case of the two-telescope coincidence, the telescopes were always pointed perpendicular to the line connecting the telescopes. Rates are relatively flat out to zenith angles of 40° . As the zenith angle increases, the

distance of showers to the telescope increases, reducing the density of photons in the light pool and hence increasing the effective energy threshold of the telescope. At the same time the diameter of the light pool and the effective area increase. The size of the images decreases, resulting in the concentration of light in fewer pixels and in more efficient triggers. For angles up to 40° , these effects more or less compensate each other, resulting in a constant rate. At larger angles, the increase in threshold - also due to atmospheric extinction - dominates. A two-telescope coincidence profits more from the enlarged light pool at non-zero zenith angles, and the drop at larger zenith angles starts later, compared to a single telescope. Simple analytical models can only approximately describe this behaviour; the dashed lines in Fig. 9 represent such an attempt.

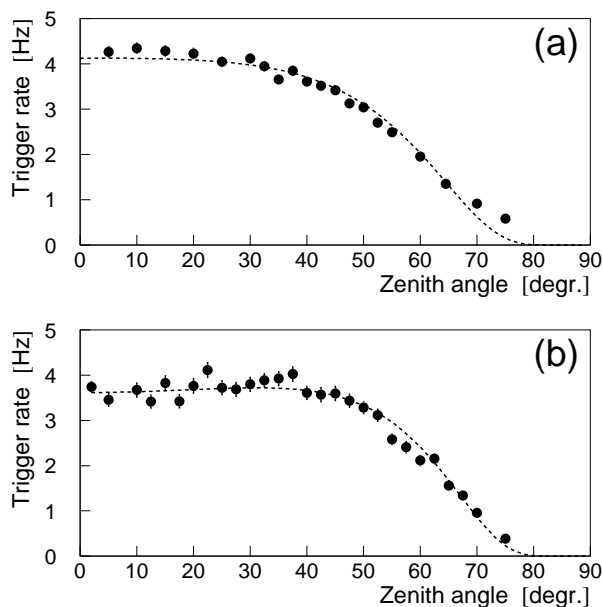


Fig. 9. Single-telescope rate (a) and coincidence rate between telescopes CT3 and CT4 (b) as a function of the zenith angle. The absolute values of the rates cannot be compared, since data were taken with a higher threshold in case of the single-telescope trigger.

6 Trigger characteristics of γ -rays as compared to cosmic rays

All measurements discussed above refer to cosmic-ray trigger rates. Of course, it is interesting to see if the trigger properties of γ -rays differ. Monte-Carlo simulations, e.g., predict that a multi-telescope coincidence suppresses cosmic rays already at the trigger level [10]. The recent flare of Mkn 501 has provided

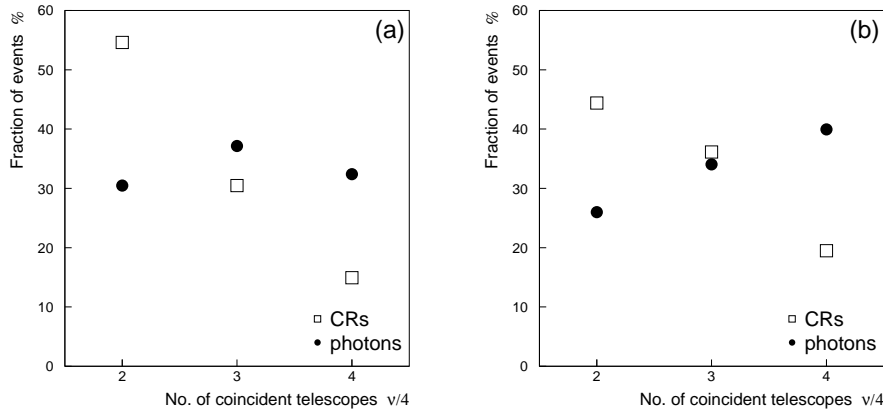


Fig. 10. Fraction of two-, three-, and four-telescope events for cosmic-ray triggers (open squares) and for γ -rays from the Mkn 501 data sample (full circles), for zenith angles between 12° to 20° (a) and between 30° to 40° (b).

a large sample a γ -rays, which can be clearly separated from cosmic rays on the basis of their direction [4]; the small cosmic-ray background under the γ -ray signal can be reliably subtracted on a statistical basis.

The flaring nature of the γ -ray emission of Mkn 501 does unfortunately not allow to compare rates measured at different times, and hence does not allow to determine unambiguously a zenith-angle dependence of γ -ray trigger rates. We will therefore limit ourselves to the discussion of the relative rates of twofold, threefold, and fourfold telescope coincidences. In order to minimize a possible selection bias, γ -rays were defined as showers within 0.32° from Mkn 501 (compared to a typical angular resolution of 0.1°), with a mean width of the images (averaged over all telescopes) not more than 40% larger than expected for γ -rays. This latter cut is more than 95% efficient. Mkn 501 data were taken with the source located 0.5° away from the center of cameras; therefore, an opposite, but otherwise equivalent region can be used to study background cosmic rays under identical conditions. The resulting relative coincidence rates are compared for γ -rays and cosmic rays in Fig. 10, for two different zenith angles. One finds that γ -ray showers tend to trigger a larger number of telescopes, as compared to cosmic-ray showers. The more telescopes are required at the trigger level, the larger is the fraction of γ -rays among the triggered events. With increasing zenith angles, the fraction of four-telescope coincidences increases and the fraction of twofold coincidences decreases, as expected due to the growing diameter of the light pool.

7 Summary

Using the HEGRA IACT system, single-telescope and multi-telescope coincidence rates were studied as a function of pixel threshold and telescope orientation, using both a standard two-pixel coincidence to trigger an individual telescope, and a topological trigger which requires neighboring trigger pixels.

The multi-telescope trigger scheme of the HEGRA IACT System allows to operate the system at a pixel threshold lower by a factor of two compared to single telescope operation with a standard two-pixel coincidence. At the system level the role of random coincidences is negligible and therefore the limiting factor for further reduction of the energy threshold is the quality of the recorded images.

Studies with the Mkn 501 γ -ray sample demonstrate that a multi-telescope trigger enhances the fraction of γ -rays in the event sample.

Acknowledgements

The support of the HEGRA experiment by the German Ministry for Research and Technology BMBF and by the Spanish Research Council CYCIT is acknowledged. We are grateful to the Instituto de Astrofisica de Canarias for the use of the site and for providing excellent working conditions. We thank the other members of the HEGRA CT group, who participated in the construction, installation, and operation of the telescopes. We gratefully acknowledge the technical support staff of Heidelberg, Kiel, Munich, and Yerevan.

REFERENCES

References

- [1] T.C. Weekes, Space Science Rev. 75 (1996) 1; M. F. Cawley and T.C. Weekes, Experimental Astronomy 6 (1996) 7.
- [2] D.J. Fegan, J. Phys. G 23 (1997) 1013.
- [3] A. Daum et al., astro-ph/9704098, Astroparticle Phys., in press.
- [4] F. Aharonian et al., astro-ph/9706019, Astron. Astrophys., in press.
- [5] G. Hermann, Proceedings of the Int. Workshop "Towards a Major Atmospheric Cherenkov Detector IV", Padua, (1995), M. Cresti (Ed.), p. 396.

- [6] C. Köhler et al., *Astropart. Phys.* 6 (1996) 77; Err. 6 (1997) 423.
- [7] G. Hermann et al., MPI H-V36-1995 (1995).
- [8] R. Mirzoyan, *Proceedings of the Int. Workshop “Towards a Major Atmospheric Cherenkov Detector IV”*, Padua, (1995), M. Cresti (Ed.), p. 209.
- [9] R. Mirzoyan, priv. comm.
- [10] F. Aharonian et al., *Astroparticle Phys.* 6 (1997) 343,